sustainability

MDPI

Article

Prediction of Energy-Related Carbon Emissions in East China Using a Spatial Reverse-Accumulation Discrete Grey Model

Shubei Wang, Xiaoling Yuan and Zhongguo Jin *

School of Economics and Finance, Xi'an Jiaotong University, Xi'an 710049, China; shubeiwang@yeah.net (S.W.); xiaoling@mail.xjtu.edu.cn (X.Y.)
* Correspondence: zhongguojin@stu.xjtu.edu.cn

Abstract: In order to better analyze and predict energy-related carbon emissions in East China to address climate change, this paper enhances the predictive capabilities of grey models in spatial joint prediction by creating the reverse-accumulation spatial discrete grey model RSDGM (1,1,m) and accumulation spatial discrete grey breakpoint model RSDGBM (1,1,m,t), which took the impact of system shocks into consideration. The efficiency of the models is confirmed by calculating the energy-related carbon emissions in East China from 2010 to 2022. Future emissions are predicted, and the spatial spillover effect of emissions in East China is discussed. The conclusions are as follows: (1) The RSDGM (1,1,m) theoretically avoids errors in background values and parameter calculations, reducing computational complexity. Empirically, the model exhibits high performance and reflects the priority of new information in spatial joint analysis. (2) The RSDGBM (1,1,m,t) captures the impact of shocks on system development, improving the reliability of carbon emissions prediction. (3) Jiangsu and Shandong are positively affected by spatial factors in terms of carbon emissions, while Shanghai and Zhejiang are negatively affected. (4) It is estimated that carbon emissions in East China will increase by approximately 23.8% in 2030 compared to the level in 2022, with the levels in Zhejiang and Fujian expected to increase by 45.2% and 39.7%, respectively; additionally, the level in Shanghai is projected to decrease. Overall, East China still faces significant pressure to reduce emissions.

Keywords: spatial correlation; reverse accumulation spatial discrete grey model; energy-related carbon emissions; carbon projections; East China region

check for updates

Citation: Wang, S.; Yuan, X.; Jin, Z. Prediction of Energy-Related Carbon Emissions in East China Using a Spatial Reverse-Accumulation Discrete Grey Model. *Sustainability* **2024**, *16*, 9428. https://doi.org/10.3390/su16219428

Academic Editors: Manuela Almeida and Ljubomir Jankovic

Received: 11 July 2024
Revised: 16 September 2024
Accepted: 28 October 2024
Published: 30 October 2024

Copyright: © 2024 by the authors. Licensee MDPI, Basel, Switzerland. This article is an open access article distributed under the terms and conditions of the Creative Commons Attribution (CC BY) license (https://creativecommons.org/licenses/by/4.0/).

1. Introduction

With the development of the global economy and industrialization, the issue of global warming has become increasingly severe. In particular, the rapid increase in carbon dioxide emissions from energy consumption activities has put significant pressure on ecosystems. Despite the world's great efforts to reduce carbon dioxide emissions, fossil fuels are still widely used across all sectors of the economy [1]. As a result, countries have focused on managing carbon dioxide and other greenhouse gas emissions and promoting the growth of a low-carbon economy. As the world's top carbon emitter and the world's second-largest economy, China has never shirked its responsibility to reduce carbon emissions [2]. Subsequent references to carbon emissions in this paper generally refer to energy-related carbon emissions. At the 75th United Nations General Assembly in 2020, President Xi Jinping declared that "China will enhance its nationally determined contributions and implement more forceful policies and measures. We aim to peak carbon emissions before 2030 and achieve carbon neutrality before 2060". Economic development causes carbon emissions, and the regional economic development in China is relatively unbalanced, so the regional carbon emissions are also unbalanced. The East China region, which is densely populated, plays a crucial role in driving China's economic growth. Nevertheless, as the East China region experiences swift economic expansion and rapid urban development,

there is also a rise in carbon emissions. Hence, it is highly practical to analyze and forecast carbon emissions in the region of East China. This study provides a scientific basis for formulating carbon emission control policies and tapping into the emission reduction potential of the East China region by forecasting its carbon emissions, which is crucial for achieving low-carbon economic development and addressing climate change.

1.1. Background

Since the 21st century, climate change has become a common threat faced by all countries in the world, and global warming caused by the massive emission of greenhouse gases, mainly carbon dioxide, has become the greatest non-traditional security challenge threatening the development of all mankind. According to the fourth synthesis assessment report released by the Intergovernmental Panel on Climate Change (IPCC) in 2007, carbon dioxide from fossil energy consumption has been a significant contributor to global warming over the past 50 years [3]. The sixth synthesis assessment report released by the IPCC in 2023 forecasts that the world's average temperature may further increase by 1.5 °C over the next 20 years [4]. How mankind can achieve sustainable economic development while controlling climate change has become an urgent problem for all countries. China's economy has been growing at a high rate since the reform and opening up. China's National Bureau of Statistics showed that the annual gross domestic product exceeded 126 trillion yuan in 2023. As the world's second-largest economy, China is an important engine of world economic growth, which is expected to contribute more than 30% to world economic growth. China's rapid economic development is inevitably accompanied by large amounts of carbon emissions from energy consumption. The BP statistical review of world energy in 2022 presents that China topped the world in carbon emissions related to energy, with a total of 10,523.03 million tons, surpassing the United States and accounting for 31% of the global total [5]. Considering the urgency and severity of climate change, the Chinese government has attached great importance to addressing carbon emissions. The 14th Five-Year Plan for a Modern Energy System explicitly outlines a goal to reduce energy consumption per unit of GDP by 13.5% and carbon dioxide emissions per unit of GDP by 18% by 2025 compared to the levels in 2020. Yang et al. (2022) took the imbalance of regional economic development and energy consumption in China into consideration and studied the carbon emissions in China's six regions from 1997 to 2017. The result showed that energy consumption was mainly derived from coal, and coal consumption was highest in the East China region [6]. The East China region, including Shanghai, Jiangsu, Zhejiang, Anhui, Fujian, Jiangxi, and Shandong, has a favorable geographic location, a strong economic base, a well-developed industrial system, and has significant advantages in the fields of high technology, financial services, and trade logistics, which makes East China one of the most economically developed regions in China. In 2023, East China ranked first among the six regions in China in terms of GDP. In short, considering the influence of East China on China's regional economic development and carbon emissions, the prediction of carbon emissions in East China is of great practical significance.

1.2. Literature Review

It is crucial for reducing the effects of uncertainty on upcoming economic activities through forecasting. Decision-makers can improve their comprehension of future events and maintain the health and stability of the economic system with the help of these predictions. Currently, various methods are employed for carbon emission forecasting, such as macroeconomic models [7,8], index decomposition models [9,10], and machine learning models [11]. Forecasting methods are utilized to investigate the undiscovered principles of system evolution using scientific principles, trustworthy information, and accurate computations. They predict the further development of a system and are necessary for promoting sustainable economic and social development. Nevertheless, a significant quantity of observational data is necessary to attain acceptable precision with these methods. In real-world scenarios, these methods may only be applicable for investigating specific principles of

system evolution due to constraints in information and understanding. In such cases, basic models can sometimes outperform intricate models, particularly when there is a lack of data, and it is not comprehensive. As a result, therefore, Deng (1982) introduced the grey system theory to predict the development trend of systems [12]. Grey forecasting models were created for time series data that have uncertainty, incomplete information, and missing data, featuring simple structures and high effectiveness. Grey forecasting models differ from linear regression, index decomposition, machine learning, and other methods by considering different factors as grey action quantities and directly modeling the research variables. These methods do not need a significant quantity of sample data for training and self-learning, and there is no need to take into account the factors that impact the model variables. Carbon emissions are greatly affected by uncertainty, and the operation of systems changes frequently. Additionally, data collection is time-intensive. In cases with data uncertainty and scarcity, grey forecasting models have been successfully applied [13–15].

The grey model has been actively explored in the field of grey system theory in recent years. It is recognized for being concise, simple to compute, and for streamlining the modeling procedure. The grey model is known for its high accuracy in modeling small samples and predicting incomplete information problems, which has garnered significant interest in mainstream prediction theory as a new research focus. However, the core model GM (1,1) has issues such as insufficient prediction accuracy and limited applicability. Scholars have enhanced the predictive accuracy of the model by optimizing the structure and parameters of the conventional grey model from various angles. These optimizations include optimization of initial values [16,17], optimization of background values [18,19], and optimization of accumulation, among other strategies. Accumulating data is a critical step in the grey model for data processing and is essential for the modeling process. Scholars have optimized and expanded the grey model by constructing different accumulation operators. For example, the original method of accumulating integers was replaced with fractional-order accumulation, enhancing the grey prediction model's effectiveness for nonexponential sequences [20]. However, due to the complexity of fractional-order accumulation and differentiation, Ma et al. (2020) proposed a more convenient conformable fractional-order accumulation operator [21]. Subsequently, scholars have proposed other accumulation operators, such as the Hausdorff fractional-order accumulation operator [22] and the weakened fractional-order accumulation operator [23]. Grey prediction models commonly utilize fractional-order accumulation operations at present. In order to give more importance to new data, Song and Deng (2001) developed an opposite-direction accumulation operator by altering the accumulation direction in the conventional GM (1,1) model [24]. In certain situations, opposite-direction accumulation can result in a more effective model than forward accumulation [25,26]. Although opposite-direction accumulation can further improve simulation performance in some cases, its characteristics lead to poor extrapolation performance. Therefore, Wang and Zhang proposed a reverse-accumulation operator and constructed the fractional grey reverse accumulation model FGRM (1,1). They then combined it with conformable fractional-order accumulation to construct the conformable fractional opposite-direction grey prediction model CFGNOM (1,1), demonstrating that reverse accumulation has better application prospects than opposite-direction accumulation [27,28]. Furthermore, in order to address the issues related to the uncertain fractional-order accumulation order, various optimization algorithms have been utilized to identify the most suitable parameter values. The moth flame optimization algorithm [29], grey wolf optimization algorithm [30], and particle swarm optimization algorithm [31] are part of these algorithms.

One of the main methods for improving the grey model is to expand the model structure. To avoid discontinuity bias in the modeling process, researchers have conducted studies on model structure from a discrete perspective [32–34]. As a result, the discrete grey model not only minimizes modeling inaccuracies but also simplifies the model to a certain degree. According to the first law of geography, there is a spatial correlation

in any economic activity. In Wang and Zhang's (2022) study, they incorporated a spatial element into the grey model to create the spatial grey model SGM (1,1,m), enhancing the predictive accuracy of the conventional model and enabling the analysis of spatial interconnections within systems [35]. Subsequently, a multivariate spatial grey model was established to obtain predictions of China's 3E system. Gao et al. (2022) proposed a novel spatiotemporal grey model for forecasting PM2.5 and found that a lockdown has a positive effect on urban air quality by quantitatively analyzing the spillover and momentum effects [36]. Based on the occurrence of the pandemic in 2020, Zhang and Wang (2023) introduced time breakpoints into the grey model to construct the grey breakpoint model GBPM (1,1,t). The results showed that the model can effectively capture shock information in the system, achieve quantitative analysis of shocks, and further expand the applicability of the traditional grey model [37]. Furthermore, scholars have enhanced the design of the grey model by focusing on enhancing grey actions [38], creating combined models [39], and optimizing Bernoulli methods [40,41]. The optimization methods not only expand the fundamental structure of grey prediction models in theory but also enhance the precision and flexibility of predictions to a certain degree.

In summary, scholars have made various improvements and optimizations to the grey model, achieving many effective advancements. The implementation of the spatial grey model has important practical consequences for predicting across multiple regions. However, there are still some shortcomings in its model construction. Initially, the current spatial grey model SGM (1,1,m) overlooks discontinuity bias in the calculation process, and the conventional method of first-order accumulation does not completely grasp the most recent system information, leading to a certain degree of impact on the predictive accuracy of the model. Furthermore, the traditional models fail to consider the influence of unexpected events on system functioning, and the undeniable effect of the COVID-19 pandemic on carbon emission systems in 2020 was highlighted by Han et al. (2021) and Shan et al. (2021) [42,43]. This makes traditional models unsuitable for carbon emission prediction work in the current environment. Hence, the RSDGM (1,1,m) was developed by incorporating the reverse-accumulation operator into the discrete spatial grey model, leveraging the strengths of both approaches. Additionally, a time dummy variable was added to the RSDGM (1,1,m) to construct the RSDGBM (1,1,m,t) to further improve predictive performance.

1.3. Contributions

The novelty of this paper is that to enhance the predictive capabilities of grey models in spatial joint prediction, the reverse-accumulation spatial discrete grey model RSDGM (1,1,m) was created, and the reverse-accumulation spatial discrete grey breakpoint model RSDGBM (1,1,m,t) was then developed to enhance predictive performance by considering the impact of system shocks. Using the energy balance tables of seven provinces in the East China region, carbon emissions in the region from 2010 to 2022 were calculated. The RSDGM (1,1,m) was then compared to the spatial grey model SGM (1,1,m), fractional discrete grey model FDGM (1,1), reverse-accumulation discrete grey model RDGM (1,1), and BP models based on the carbon emission data in the East China region. Predictions for future carbon emissions in the East China region were made utilizing the RSDGM (1,1,m) and RSDGBM (1,1,m,t). The primary findings and contributions of this research are outlined below:

(1) By leveraging the advantages of the discrete grey model and the reverse-accumulation operator, a reverse-accumulation spatial discrete grey model, RSDGM (1,1,m), is developed, and it enhances modeling performance by prioritizing new information.
(2) Building upon the RSDGM (1,1,m), a virtual time variable is added to develop a reverse-accumulation spatial discrete grey breakpoint model, RSDGBM (1,1,m,t). This modification makes the model more suitable for predicting system behavior in shock environments.

(3) The carbon emissions in the seven provinces of the East China region from 2010 to 2022 are calculated. Based on these estimates, the RSDGM (1,1,m) and RSDGBM (1,1,m,t) are compared to the SGM (1,1,m), FDGM (1,1), RDGM (1,1), and BP models. The results of the comparison verify the rationality of the optimization method proposed in this paper.

(4) Using the RSDGM (1,1,m) and RSDGBM (1,1,m,t), carbon emissions in the East China region from 2023 to 2030 are predicted. Additionally, the spatial spillover effect of carbon emissions in the seven provinces of the East China region is explored. These findings provide a scientific basis for formulating carbon emission control policies in the East China region.

The remainder of this paper is organized as follows. In Section 2, the SGM (1,1,m) and its optimization process are presented, focusing on the model structure and accumulation method. Additionally, the RSDGM (1,1,m) and RSDGBM (1,1,m,t) are developed. In Section 3, calculations of the carbon emissions in the East China region between 2010 and 2022 are performed, and the validity of the suggested RSDGM (1,1,m) and RSDGBM (1,1,m,t) is verified by using carbon emission data. Predictions have been made for the carbon emissions in the East China region from 2023 to 2030. In Section 4, the conclusions are presented. In Section 5, policy implications are listed.

2. Construction of the Reverse-Accumulation Spatial Discrete Grey Model

The theory of spatial correlation suggests that the characteristic variables of a particular region may be impacted, either positively or negatively, by the characteristic variables of neighboring regions. In other words, spatial correlation leads to a spatial spillover effect that significantly impacts changes in economic indicators. Therefore, it is crucial to consider spatial correlation when constructing models. This section begins by introducing the spatial grey model SGM (1,1,m), which is then optimized and improved by incorporating an accumulative method and adjusting the model structure. This results in the creation of the RSDGM (1,1,m) and RSDGBM (1,1,m,t), which further enhance the overall performance of the traditional model.

2.1. Spatial Grey Model SGM (1,1,m)

The original data matrix is denoted as $X^{(0)} = \left[X_1^{(0)}, X_2^{(0)}, \cdots, X_m^{(0)}\right]^T$, where $X_j^{(0)} = (x_j^{(0)}(1), x_j^{(0)}(2), \cdots, x_j^{(0)}(n))$ and $j = 1, 2, \cdots, m$. m represents the number of spatial units, n represents the time series length, and T is the transpose symbol. The data representation of all spatial units in the period k is denoted as $X^{(0)}(k) = (x_1^{(0)}(k), x_2^{(0)}(k), \cdots, x_m^{(0)}(k))^T$, and thus, the original data can also be represented as $X^{(0)} = \left[X^{(0)}(1), X^{(0)}(2), \cdots, X^{(0)}(n)\right]$. The first-order accumulation matrix of the original data is denoted as $X^{(1)} = \left[X^{(1)}(1), X^{(1)}(2), \cdots, X^{(1)}(n)\right]$, where

$$X^{(1)}(k) = (x_1^{(1)}(k), x_2^{(1)}(k), \cdots, x_m^{(1)}(k))^T = \sum_{i=1}^{k} X^{(0)}(i), k = 1, 2, \cdots, n \tag{1}$$

If there is spatial correlation in the system, then

$$\frac{dX^{(1)}(t)}{dt} = AX^{(1)}(t) + BWX^{(1)}(t) + C$$
$$A = \begin{pmatrix} a_1 & 0 & \cdots & 0 \\ 0 & a_2 & \cdots & 0 \\ \vdots & \vdots & \ddots & \vdots \\ 0 & 0 & \cdots & a_m \end{pmatrix}, B = \begin{pmatrix} b_1 & 0 & \cdots & 0 \\ 0 & b_2 & \cdots & 0 \\ \vdots & \vdots & \ddots & \vdots \\ 0 & 0 & \cdots & b_m \end{pmatrix}, C = (c_1, c_2, \cdots, c_m)T \tag{2}$$

is referred to as the differential equation of the spatial grey model SGM (1,1,m), where the term $WX^{(1)}(t)$ represents the endogenous interaction effects between different spatial units; i.e., the spatial lag term of the sequence $X^{(1)}(t)$. $W = \left[w_{ij}\right]_{m\times m}$ is the spatial weight matrix with a main diagonal of 0 and is symmetric. Matrix A is the matrix of development coefficients, and matrix B is the matrix of spatial correlation coefficients. Vector C represents the vector of grey action quantities. By solving the basic form of the model, the time response of the model can be obtained as

$$\begin{gathered}\hat{X}^{(1)}(k) = e^{D(t-1)}(X^{(1)}(1) + D^{-1}C) - D^{-1}C, k = 1, 2, \cdots, n \\ D = (A + BW)\end{gathered} \tag{3}$$

Therefore, the final restoration equation of the model can be derived as

$$\begin{gathered}\hat{X}^{(0)}(1) = \hat{X}^{(1)}(1) \\ \hat{X}^{(0)}(k) = \hat{X}^{(1)}(k) - \hat{X}^{(1)}(k-1), k = 2, 3, \cdots, n\end{gathered} \tag{4}$$

The background value matrix of $X^{(1)}$ can be represented by matrix $Z^{(1)} = (Z^{(1)}(2), Z^{(1)}(3), \cdots, Z^{(1)}(n))$, and by integrating both sides of the model over the interval $[k-1, k]$, the basic form of the model can be obtained as

$$\begin{gathered}X^{(0)}(k) = AZ^{(1)}(k) + BWZ^{(1)}(k) + C, k = 2, 3, \cdots, n \\ Z^{(1)}(k) = \alpha X^{(1)}(k) + (1-\alpha)X^{(1)}(k-1), \alpha \in [0, 1]\end{gathered} \tag{5}$$

Let $Q^{(1)} = WZ^{(1)} = \left[q_j^{(1)}(k)\right]_{m\times n-1}$. Then, the parameter vector $p_j = (a_j, b_j, c_j)T$, $j = 1, 2, \cdots, m$ can be obtained using the least squares method.

$$\begin{gathered}p_j = (a_j, b_j, c_j)T = (H_j^T H_j)^{-1} H_j^T Y_j \\ H_j = \begin{bmatrix} z_j^{(1)}(2) & q_j^{(1)}(2) & 1 \\ z_j^{(1)}(3) & q_j^{(1)}(3) & 1 \\ \vdots & \vdots & \vdots \\ z_j^{(1)}(n) & q_j^{(1)}(n) & 1 \end{bmatrix} = \begin{bmatrix} (Z_j^{(1)})T & (Q_J^{(1)})T & I_{(n-1)\times 1} \end{bmatrix},\ Y_j = \begin{bmatrix} x_j^{(0)}(2) \\ x_j^{(0)}(3) \\ \vdots \\ x_j^{(0)}(n) \end{bmatrix}\end{gathered} \tag{6}$$

According to the model establishment process described above, several deficiencies can be identified. Firstly, the calculation of the background value matrix $Z^{(1)}$ is based on an approximate solution, and errors in the calculation of the background value lead to modeling errors. Additionally, the selection of the background value coefficient α is complex, limiting the practical application of the model. Then, the time response is determined using the derivative form of the model, and the model's parameters are derived using the least squares method with respect to the model's fundamental form. This leads to inadequate alignment between the model parameters and the time response. Finally, the model continues to rely on conventional first-order accumulation for modeling, neglecting to incorporate the principle of prioritizing new information and not fully leveraging the newest data available in the system. This may lead to biases in the prediction results, especially considering the occurrence of the 2020 pandemic, which highlights the importance of new information.

2.2. Reverse-Accumulation Spatial Discrete Grey Model (RSDGM (1,1,m))

After examining the shortcomings of the SGM (1,1,m) in the preceding section and taking into account the benefits of conventional grey discrete models as well as the effective use of fractional-order accumulation in grey models, a simple enhancement to the model's

structure is suggested. Through restructuring the basic structure of the SGM (1,1,m), we are able to obtain

$$(I - \alpha A)X^{(1)}(k) = (I + (1-\alpha)A)X^{(1)}(k-1) + BW(\alpha X^{(0)}(k) + X^{(1)}(k-1)) + C \quad (7)$$

where I represents the identity matrix. The above equation directly reflects the relationship between $X^{(1)}(k)$ and $X^{(1)}(k-1)$. By approximating the term $(\alpha X^{(0)}(k) + X^{(1)}(k-1))$ as $X^{(1)}(k)$, we can derive the discrete form of the spatial grey model.

$$X^{(1)}(k) = (I - \alpha A)^{-1}(I + (1-\alpha)A)X^{(1)}(k-1) + (I - \alpha A)^{-1}BWX^{(1)}(k) + (I - \alpha A)^{-1}C \quad (8)$$

To further reflect the principle of prioritizing new information, the reverse-accumulation operator is introduced to construct the reverse-accumulation spatial discrete grey model (RSDGM (1,1,m)). The specific process of model establishment is as follows.

Let the original data matrix be denoted as $X^{(0)} = \left[X^{(0)}(1), X^{(0)}(2), \cdots, X^{(0)}(n)\right]$, which is the same definition as the matrix used in the SGM (1,1,m). Then, the r-th order reverse-accumulation matrix of the original data is denoted as $X^{(r)} = \left[X^{(r)}(1), X^{(r)}(2), \cdots, X^{(r)}(n)\right]$, where

$$X^{(r)}(k) = (x_1^{(r)}(k), x_2^{(r)}(k), \cdots, x_m^{(r)}(k))^T = \sum_{i=1}^{k} \frac{\Gamma(\alpha + i - 1)}{\Gamma(i)\Gamma(\alpha)} X^{(0)}(i), k = 1, 2, \cdots, n \quad (9)$$

If there is spatial correlation in the system, then

$$X^{(r)}(k) = AX^{(r)}(k-1) + BWX^{(r)}(k) + C$$
$$A' = \begin{pmatrix} a'_1 & 0 & \cdots & 0 \\ 0 & a'_2 & \cdots & 0 \\ \vdots & \vdots & \ddots & \vdots \\ 0 & 0 & \cdots & a'_m \end{pmatrix}, B' = \begin{pmatrix} b'_1 & 0 & \cdots & 0 \\ 0 & b'_2 & \cdots & 0 \\ \vdots & \vdots & \ddots & \vdots \\ 0 & 0 & \cdots & b'_m \end{pmatrix}, C' = (c'_1, c'_2, \cdots, c'_m)T \quad (10)$$

is the fundamental form of the reverse-accumulation spatial discrete grey model RSDGM (1,1,m), where the definitions of matrices A', B', and C' are consistent with those of matrices A, B, and C in the SGM (1,1,m). The upper-right subscript is used only for the convenience of distinction. W represents the spatial weight matrix. By organizing the basic form of the model, we can derive

$$X^{(r)}(k) = (I - B'W)^{-1}A'X^{(r)}(k-1) + (I - B'W)^{-1}C \quad (11)$$

By applying the above formula and setting $X^{(r)}(1)$ as the initial point of the model, we can derive the time response equation of the model as

$$\begin{aligned} &\hat{X}^{(r)}(k+1) = R^k X^{(r)}(1) + (I - R^k)(I - R)^{-1}G, k = 1, 2, \cdots, n \\ &R = (I - B'W)^{-1}A', G = (I - B'W)^{-1}C \end{aligned} \quad (12)$$

Finally, based on the restoration calculation of the reverse accumulation operator, the final restoration equation of the model can be inferred as

$$\hat{X}^{(0)}(k) = \frac{\Gamma(k)\Gamma(\alpha)}{\Gamma(\alpha + k - 1)}(\hat{X}^{(r)}(k) - \hat{X}^{(r)}(k-1)), k = 1, 2, 3, \cdots, n \quad (13)$$

Let $V^{(r)} = WX^{(r)} = \left[v_j^{(r)}(k)\right]_{m\times n}$. Then, according to the least squares method, we can estimate the parameter series $p'_j = (a'_j, b'_j, c'_j)^T$, where $j = 1, 2, \cdots, m$.

$$p'_j = (a'_j, b'_j, c'_j)T = (P_j^T P_j)^{-1} U_j^T U_j$$
$$P_j = \begin{bmatrix} x_j^{(r)}(1) & v_j^{(r)}(2) & 1 \\ x_j^{(r)}(2) & v_j^{(r)}(3) & 1 \\ \vdots & \vdots & \vdots \\ x_j^{(r)}(n-1) & v_j^{(r)}(n) & 1 \end{bmatrix}, \; U_j = \begin{bmatrix} x_j^{(r)}(2) \\ x_j^{(r)}(3) \\ \vdots \\ x_j^{(r)}(n) \end{bmatrix} \tag{14}$$

2.3. Model Breakpoint Optimization

The unexpected outbreak of the COVID-19 pandemic in 2020 greatly affected the operations of the economy, introducing new obstacles to predictive analysis. As a result, this paper builds upon the work of Wang and Zhang (2023) [37] by incorporating dummy variables into the RSDGM (1,1,m) to capture the changes in system operation before and after a shock. With this improvement, the RSDGBM (1,1,m,t) is developed, further enhancing the predictive accuracy of the RSDGM (1,1,m).

The original data matrix is denoted as $X^{(0)}$, and the reverse-accumulation matrix of order r is denoted as $X^{(r)}$, as defined in the previous section. Suppose that at time point t, the system operation is subject to a certain shock, and the impact of this shock on the system continuously changes as time progresses. Then,

$$X^{(r)}(k) = A'X^{(r)}(k-1) + B'WX^{(r)}(k) + \phi T(k) + C'$$
$$\phi = \begin{pmatrix} \varphi_1 & 0 & \cdots & 0 \\ 0 & \varphi_2 & \cdots & 0 \\ \vdots & \vdots & \ddots & \vdots \\ 0 & 0 & \cdots & \varphi_m \end{pmatrix}, T(k) = \begin{cases} [0]_{m,1}, k \le t \\ [k-t]_{m,1}, k > t \end{cases} \tag{15}$$

is a reverse-accumulation spatial discrete grey breakpoint model RSDGBM (1,1,m,t), where ϕ is the impact coefficient matrix, which represents the degree of impact on different regions. T is a virtual variable, and $[i]$ represents a matrix full of i entries. Before the impact occurs, T is a zero matrix. After the impact occurs, T continuously increases with time to reflect the changing impact on the system. Given the initial point of the model as $X^{(r)}(1)$, the time response of the model can be calculated as follows.

$$\hat{X}^{(r)}(k+1) = R^k X^{(r)}(1) + \sum_{i=0}^{k-1} R^i \Phi T(k+1-i) + (I - R^k)(I - R)^{-1} G$$
$$R = (I - B'W)^{-1} A', \Phi = (I - B'W)^{-1}\phi, G = (I - B'W)^{-1} C \tag{16}$$

According to the least squares method, the calculation of the column parameters $p\prime_j = (a'_j, b'_j, c'_j)^T$, where $j = 1, 2, \cdots, m$, is modified as follows.

$$p'_j = (a'_j, b'_j, \varphi_1, c'_j)T = (P'^T_j P'_j) {-1} U_j^T U_j$$
$$P'_j = \begin{bmatrix} x_j^{(r)}(1) & v_j^{(r)}(2) & 0 & 1 \\ x_j^{(r)}(2) & x_j^{(r)}(3) & 0 & 1 \\ \vdots & \vdots & \vdots & \vdots \\ x_j^{(r)}(t) & x_j^{(r)}(t+1) & 1 & 1 \\ \vdots & \vdots & \vdots & \vdots \\ x_j^{(r)}(n-1) & v_j^{(r)}(n) & n-t & 1 \end{bmatrix}, \; U_j = \begin{bmatrix} x_j^{(r)}(2) \\ x_j^{(r)}(3) \\ \vdots \\ x_j^{(r)}(n) \end{bmatrix} \tag{17}$$

The properties of the RSDGBM (1,1,m,t) can be expressed as follows:

(1) When ϕ = [0], the model degenerates into the reverse-accumulation discrete grey model RSDGM (1,1,m).
(2) When r = 1 and ϕ = [0], the model degenerates into the spatial discrete grey model SDGM (1,1,m).
(3) When B' = [0] and ϕ = [0], the model degenerates into the reverse-accumulation discrete grey model RDGM (1,1).
(4) When r = 1, B' = [0], and ϕ = [0], the model degenerates into the standard discrete grey model DGM (1,1).

Based on the definitions of the RSDGM (1,1,m) and RSDGBM (1,1,m,t) above, the following observations can be made: (1) The RSDGM (1,1,m) avoids the calculation of the background value matrix $Z^{(1)}$ and reduces the computational complexity of the traditional model by transforming it from a differential form to a discrete form. Theoretically, this enhancement boosts the model's performance in modeling and accuracy in prediction. (2) Utilizing the spatial grey model along with the reverse-accumulation operator when developing the spatial prediction equation demonstrates the importance of giving precedence to fresh data. This improvement slightly enhances the model's ability to predict outcomes. (3) The inclusion of the virtual variable T in the RSDGBM (1,1,m,t) allows it to capture the impact of system shocks. As a result, the model yields improved system predictions after a shock.

2.4. Calculation of Model Hyperparameters

In the previous section, the calculations of the development coefficient, spatial correlation coefficient, impact coefficient, and grey action term of the model were presented. However, the selection of the reverse-accumulation order r was not described. Different values of r will result in different accumulation sequences, which will affect the performance of the model. Hence, it is essential to choose a dependable sequence of accumulation. Various optimization algorithms, such as moth flame optimization (MFO), grey wolf optimization (GWO), and particle swarm optimization (PSO), are available for determining the best solution for r. In this paper, the PSO algorithm is applied to determine the accumulation order r in the RSDGBM (1,1,m,t). This method of selection relies on minimizing the mean absolute percentage error (MAPE) of the modeling samples. Figure 1 displays the sequence of the algorithm. The specific function is established as follows:

$$\min MAPE = \frac{1}{n \times m} \sum_{j=1}^{m} \sum_{k=1}^{n} \left| \frac{\hat{x}_j^{(0)}(k) - x_j^{(0)}(k)}{x_j^{(0)}(k)} \right| \times 100\% \tag{18}$$

$$s.t. \begin{cases} X^{(r)}(k) == \sum_{i=1}^{k} \frac{\Gamma(\alpha + i - 1)}{\Gamma(i)\Gamma(\alpha)} X^{(0)}(i), k = 1, 2, \cdots, n \\ X^{(r)}(k) = A' X^{(r)}(k-1) + B' W X^{(r)}(k) + \phi T(k) + C' \\ p'_j = \left(P'^T_j P'_j\right)^{-1} U_j^T U_j \\ \hat{X}^{(r)}(k+1) = R^k X^{(r)}(1) + \sum_{i=0}^{k-1} R^i \Phi T(k+1-i) + (I - R^k)(I - R)^{-1} G \\ R = (I - B'W)^{-1} A', \Phi = (I - B'W)^{-1} \phi, G = (I - B'W)^{-1} C \\ \hat{X}^{(0)}(k) = \frac{\Gamma(k)\Gamma(\alpha)}{\Gamma(\alpha + k - 1)} (\hat{X}^{(r)}(k) - \hat{X}^{(r)}(k-1)), k = 1, 2, 3, \cdots, n \end{cases} \tag{19}$$

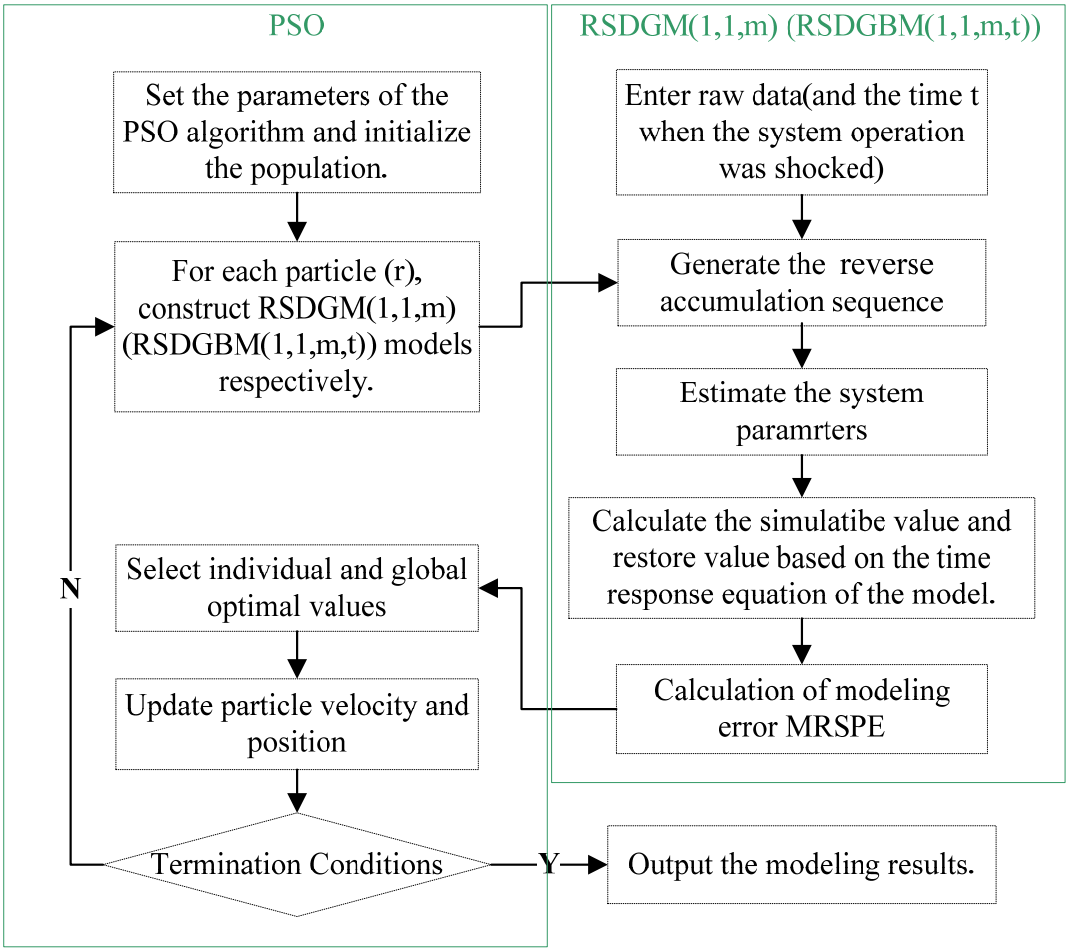


Figure 1. Flowchart of the RSDGM (1,1,m) and RSDGBM (1,1,m,t).

2.5. Flowchart of the RSDGM (1,1,m) and RSDGBM (1,1,m,t)

To illustrate the modeling process of the RSDGM (1,1,m) and RSDGBM (1,1,m,t), the modeling flowchart is shown in Figure 1.

2.6. Establishment of Evaluation Indicators

In order to confirm the dependability and appropriateness of the grey model put forth in this paper, we opted to use the enhanced MAPE for assessment. The conventional MAPE can only reflect the modeling outcomes for a single spatial unit, which would be impractical for the model in this paper if applied to each individual spatial unit. Hence, we enhanced the MAPE in this paper. Since the evaluation of grey model performance encompasses both simulation and prediction, it is necessary to calculate the errors for simulation, prediction, and overall performance. The calculation method is as follows:

Mean relative simulation percentage error (MRSPE)

$$MRSPE = \frac{1}{n \times m} \sum_{j=1}^{m} \sum_{k=1}^{n} \left| \frac{x_j^{(0)}(k) - \hat{x}_j^{(0)}(k)}{x_j^{(0)}(k)} \right| \times 100\% \tag{20}$$

Mean relative forecast percentage error (MRFPE)

$$MRFPE = \frac{1}{f \times m} \sum_{j=1}^{m} \sum_{k=n+1}^{n+f} \left| \frac{x_j^{(0)}(k) - \hat{x}_j^{(0)}(k)}{x_j^{(0)}(k)} \right| \times 100\% \tag{21}$$

Composite mean relative percentage error (CMRPE)

$$CMRPE = \frac{1}{(n+f) \times m} \sum_{j=1}^{m} \sum_{k=1}^{n+f} \left| \frac{x_j^{(0)}(k) - \hat{x}_j^{(0)}(k)}{x_j^{(0)}(k)} \right| \times 100\% \quad (22)$$

In the functions above, n represents the modeling interval, and f represents the forecasting interval.

To assess the impact of adding dummy variables on the modeling performance of the RSDGBM (1,1,m,t), the simulation errors after the breakpoints are calculated to facilitate comparative analysis. The after-breakpoint mean relative simulation percentage error (ABMRSPE) is expressed as follows:

$$ABMRSPE = \frac{1}{(n-t) \times m} \sum_{j=1}^{m} \sum_{k=t+1}^{n} \left| \frac{x_j^{(0)}(k) - \hat{x}_j^{(0)}(k)}{x_j^{(0)}(k)} \right| \times 100\% \quad (23)$$

In addition, the article further evaluates the modeling results using R^2 to facilitate better comparison with other studies. The R^2 calculation formula for the modeling results is as follows:

$$R^2 = mean({R^2}_j) = 1 - \frac{1}{m} \sum_{j=1}^{m} \frac{\sum_{k=1}^{n} \left(x_j^{(0)}(k) - \hat{x}_j^{(0)}(k) \right)^2}{\sum_{k=1}^{n} \left(x_j^{(0)}(k) - \overline{x}_j^{(0)} \right)^2} \quad (24)$$

3. Prediction of Carbon Emissions in the East China Region

The analysis process of carbon emissions in the East China region is shown in Figure 2 of this paper. Initially, the carbon emissions in the East China region from 2010 to 2022 are calculated, followed by the recognition of spatial connections between carbon emissions in various provinces and urban areas. Next, the proposed RSDGM (1,1,m)'s effectiveness is confirmed by comparing it with the benchmark model. Finally, the RSDGM (1,1,m) and RSDGM (1,1,m,t) have been created to predict carbon emissions in the East China region from 2023 to 2030 and examine the spatial ripple effects of these emissions.

3.1. Calculation of Carbon Emissions in the East China Region

To ensure maximum accuracy, the calculation of carbon dioxide emissions requires fuel consumption calculations for different selected fossil fuels. Therefore, first, fossil fuel consumption calculations are performed for carbon emissions accounting. Following this, the East China region's carbon emissions are assessed by the amount of fossil fuels consumed. To obtain energy consumption data, the approach used by Liang et al. (2021) is adopted [44], and regional energy balance sheets are used to account for interprovincial energy consumption variations. An energy balance sheet is a matrix that summarizes data on the supply, processing, conversion, and final consumption of various types of energy. It provides an intuitive representation of the flows among different energy types and the energy balance. In this study, only the processing and conversion data, as well as the final consumption data, are considered. The data of energy balance sheets of the seven provinces in the East China region from 2010 to 2022 were extracted from the "*China Energy Statistical Yearbook*" covering the period from 2011 to 2023.

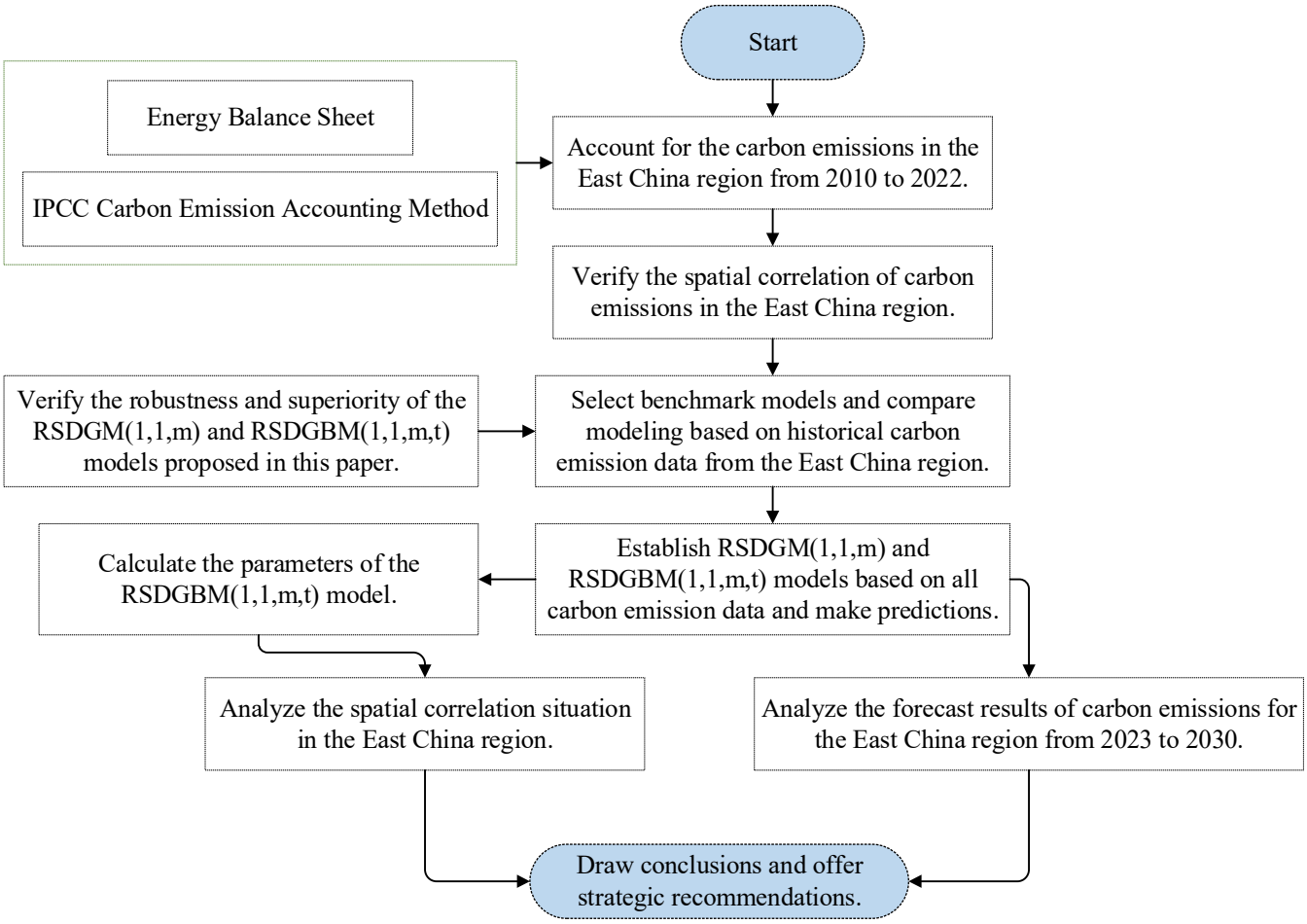


Figure 2. Article Analysis Flowchart.

The accounting of energy consumption requires determining the types of energy to be included in the calculation and processing of the consumption data for individual energy sources in the energy balance sheet. To ensure accuracy, all primary or secondary energy sources used for combustion must be included in the accounting of energy consumption. Selecting only a few major energy sources would result in the underestimation of energy consumption, while selecting all energy types would result in the overestimation of energy consumption. For example, energy sources such as naphtha, lubricating oil, and paraffin are not used for combustion, and the accounting process for thermal and electrical energy differs due to the different energy sources used in processing and conversion. For optimal precision, 14 energy sources are chosen from the energy balance sheet for calculation: coal, coke, coke oven gas, blast furnace gas, converter gas, other gases, crude oil, gasoline, kerosene, diesel, fuel oil, liquefied petroleum gas, natural gas, and liquefied natural gas. When selecting the consumption data for individual energy sources, using the total energy consumption data directly would result in the double counting of secondary energy consumption. Additionally, using only the final consumption would include the portions of energy used to process raw materials and industrial production, leading to the underestimation of electricity and heat energy consumption. To obtain accurate net consumption values for individual energy sources, the consumption data for individual energy sources in the energy balance sheet needs to be processed. In this study, the net consumption of individual energy sources is calculated by subtracting the portions of raw materials and materials used in industrial production from the final consumption value and then adding the energy inputs for electricity and heat. This calculation excludes the inputs from secondary energy conversion, avoids the double counting of certain types of energy consumption, and yields an accurate estimate of the net consumption of individual energy sources in relation to

carbon dioxide emissions. Finally, based on a total of 91 energy balance sheets from 2010 to 2022 for each province, the net consumption of 14 energy sources in each province over these 13 years was obtained by processing the data for various energy sources year by year and province by province.

The 2006 IPCC National Greenhouse Gas Inventory Guidelines offer detailed explanations of three methods for calculating carbon dioxide emissions. Method 1, which is widely adopted by most scholars, is utilized in this paper. In this approach, carbon dioxide emissions are calculated by considering energy consumption and carbon dioxide emission factors for each energy source. The specific calculation method is as follows:

$$CE_{i,t} = \sum_{j=1}^{14} EC_{i,j,t} \times NCV_j \times EF_j \tag{25}$$

In this equation, i stands for different provinces, j stands for different fossil fuels, t stands for time, $EC_{i,j,t}$ stands for the net consumption of the j-th type of energy in province i at time t, and $CE_{i,t}$ stands for the carbon dioxide emissions in province i at time t. NCV_j stands for the average minimum heating value of the j-th energy source. The data are obtained from the "*China Energy Statistical Yearbook 2022*", with coal values based on raw coal data and average values used for other gases. The stats of blast furnace gas, converter gas, and liquefied natural gas are obtained from the "Statistical System for Energy Resource Consumption in Public Institutions". EF_j stands for the effective carbon dioxide emission factor for the jth energy source, and the specific calculation method is as follows:

$$EF_j = CC_j \times COF_j \times {}^{44}/_{12} \tag{26}$$

In this equation, CC_j stands for the default carbon content of energy source j based on data from the "IPCC National Greenhouse Gas Inventory Guidelines". For coal, the average values for anthracite coal, coking coal, other bituminous coal, subbituminous coal, and lignite are used. For converter gas, the value of the oxygen-blown converter gas from steelmaking is considered. The other gases had the same carbon content as coke oven gas. COF_j is the carbon oxidation factor for energy source j. According to the IPCC guidelines, this value is usually set to 1, indicating complete oxidation of the energy source. The ratio of the molecular weight of carbon dioxide to that of carbon is 44/12.

In Figure 3, the carbon emissions of the seven provinces in the East China region are calculated. In terms of the regional proportion, over 50% of total carbon emissions in the East China region were concentrated in Jiangsu and Shandong provinces. In terms of temporal changes, over the period from 2010 to 2022, there was a general rise in carbon emissions in the East China region. Jiangxi and Anhui provinces experienced the largest increase in carbon emissions, with growth rates of 70.3% and 54.5%, respectively. On the other hand, carbon emissions in Shanghai and Zhejiang have remained relatively stable, especially prior to 2019, with the carbon emissions curve maintaining a relatively flat trend. In fact, carbon emissions in Shanghai have even decreased to some extent. The outbreak of COVID-19 in 2020 led to a notable reduction in carbon emissions, particularly in Shanghai, Jiangsu, and Zhejiang, where a substantial decline was observed. Subsequently, there was a noticeable rebound in carbon emissions in places like Zhejiang and Fujian.

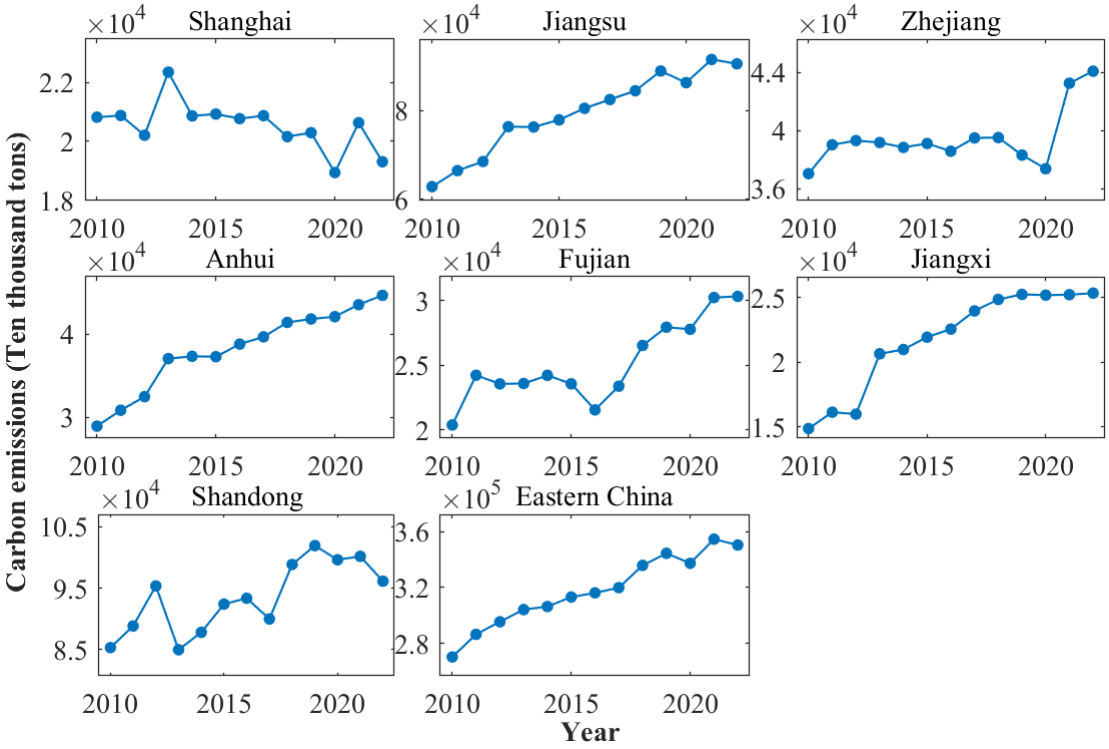


Figure 3. Carbon emissions in the East China region from 2010 to 2022.

3.2. Spatial Correlation Test of Carbon Emissions

This study utilizes an exploratory spatial data analysis technique to investigate the spatial relationship of carbon emissions through the global Moran's I index. Prior to performing the correlation test, it is necessary to establish a spatial weight matrix, typically in the form of either a spatial adjacency matrix or a spatial geographic distance matrix. For ease of calculation, the spatial adjacency matrix is used for the correlation test in this study as follows:

$$w_{ij}\begin{cases} 1 \; If \; i \; and \; j \; are \; adjacent \\ 0 \quad Other \end{cases} \tag{27}$$

where i and j stand for the province numbers. The results of the spatial autocorrelation test are shown in Table 1. From 2010 to 2022, all Moran's I values were greater than 0 and statistically significant at the 10% level. Although a Z-value less than 1.65 indicates no apparent clustering characteristics among carbon emissions, a p-value less than 0.1 has confirmed the existence of spatial correlation in carbon emissions between different provinces. Therefore, utilizing the spatial grey model is a logical approach for forecasting carbon emissions in the eastern region of China.

Table 1. Global Moran's I for carbon emissions in the East China region from 2010 to 2022.

Year	Moran's I	Z-Score	*p*-Value	Year	Moran's I	Z-Score	*p*-Value
2010	0.150	1.559	0.060	2017	0.180	1.586	0.056
2011	0.136	1.484	0.069	2018	0.180	1.615	0.053
2012	0.147	1.564	0.059	2019	0.182	1.617	0.053
2013	0.186	1.616	0.053	2020	0.183	1.625	0.052
2014	0.179	1.598	0.055	2021	0.158	1.485	0.069
2015	0.177	1.606	0.054	2022	0.147	1.428	0.077
2016	0.194	1.671	0.047				

3.3. Model Performance Evaluation

Initially, a model is created using carbon emission data from seven provinces in the East China region from 2010 to 2018 to predict the period of 2019. Considering the changes in the carbon emission landscape after 2019, this section does not include predictions for the period following 2019. The simulation and predictive performance of the RSDGM (1,1,m) and RSDGBM (1,1,m,t) are compared with those of various benchmark models to validate their superiority. In the RSDGBM (1,1,m,t), based on the judgment of the original data, the year 2013 is taken as the breakpoint t. The SGM (1,1,m) is chosen as the reference model for evaluating and validating the benefits of model discretization and reverse-accumulation optimization. The FDGM (1,1) and RDGM (1,1) are chosen to evaluate the rationality of the spatial terms of the proposed model. A BP neural network model is employed to assess and validate the predictive performance of the grey model. For convenience, the abbreviations used in the subsequent text are RSDGBM, RSDGM, SGM, FDGM, RDGM, and BP. The model calculations are conducted using MATLAB software (Version: R2021a).

Each model utilizes the PSO algorithm for hyperparameter selection. The PSO algorithm is set up with the following parameters: learning factors c1 = c2 = 2, population size = 50, maximum number of iterations = 200, accumulation order values ranging from 0 to 3, and background value coefficient values ranging from 0 to 1. The PSO algorithm iteration process for the four grey models is depicted in Figure 4. The PSO algorithm successfully selects the optimal hyperparameters for the five grey models after approximately 50 iterations. This demonstrates the successful application of the PSO algorithm in hyperparameter selection for grey models. Based on the results of the PSO algorithm, the optimal accumulation orders for the RSDGBM, RSDGM, RDGM, and FDGM are 1.1326, 0.9018, 0.9498, and 0, respectively, and the optimal background value coefficient for the SGM is 0.4631.

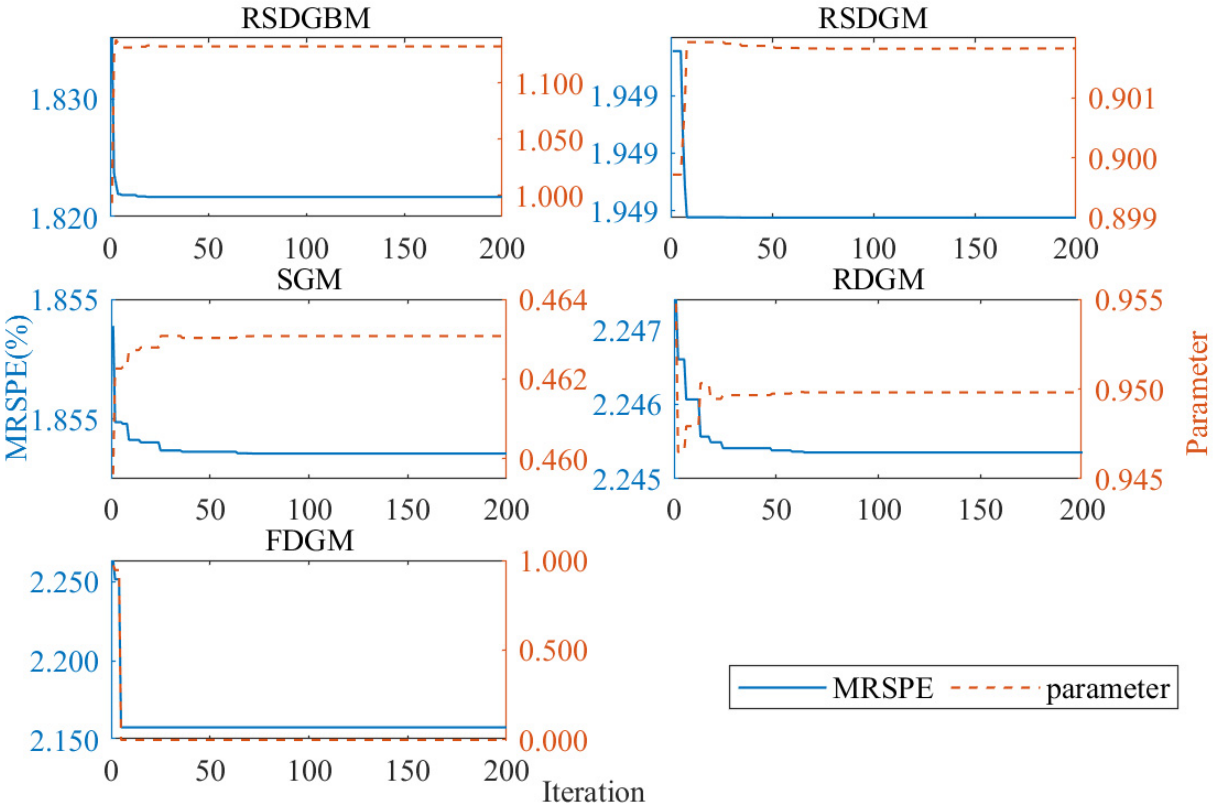


Figure 4. Iteration process of the PSO algorithm in model evaluation.

The modeling error of each model is presented in Figure 5. Initially, the RSDGBM boasts the highest R-squared value and the lowest MRSPE and MRFPE, indicative of its exemplary modeling performance. When comparing the RSDGM and SGM, it is observed that although the SGM yields a smaller MRSPE, the RSDGM yields smaller MRFPE and CMRPE values. This suggests that the RSDGM outperforms the SGM in terms of overall modeling performance, indicating the reasonableness of the optimization method used for model discretization and reverse accumulation. In addition, RSDGBM and RSDGM outperform the FDGM and RDGM when considering all three error indicators, with an MRFPE of less than 4%, demonstrating that considering spatial correlation in grey models can lead to a notable enhancement in predictive accuracy. In contrast, the BP model exhibits larger modeling errors than the four grey models. This suggests that grey models are more suitable for cases with spatial correlation and small sample sizes.

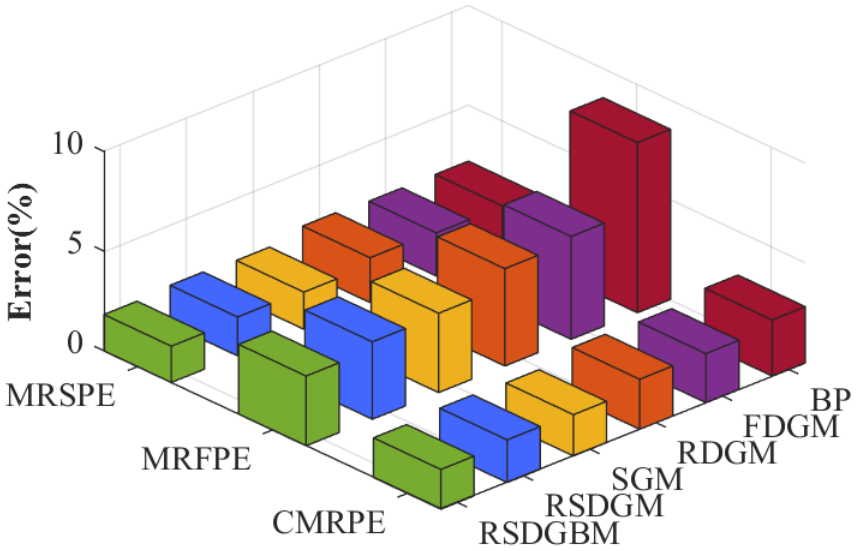


Figure 5. Modeling errors of different models.

Figure 6 displays the outcomes of the modeling for each model, while Figure 7 shows the fitting of the original data at different time points. The BP model exhibits a high degree of randomness in its modeling results, deviating significantly from the original data, particularly in regions such as Shanghai, Fujian, and Shandong. The FDGM and RDGM yield very similar results, with their curves almost overlapping. However, both models fail to capture the latest development trend of the system, especially in Anhui and Jiangxi, where they do not account for the slowdown in carbon emission growth. Instead, their predicted results continue to follow the original growth pattern. The SGM stands out from the other models, primarily in the Shanghai region, where its predicted results reflect an excessive downward trend in carbon emissions, and this overestimation is reflective of overfitting. On the other hand, RSDGBM and RSDGM demonstrate excellent performance by accurately capturing recent changes in the system. It demonstrates a strong correlation with the data at every time point, especially in areas like Shanghai, Fujian, and Shandong.

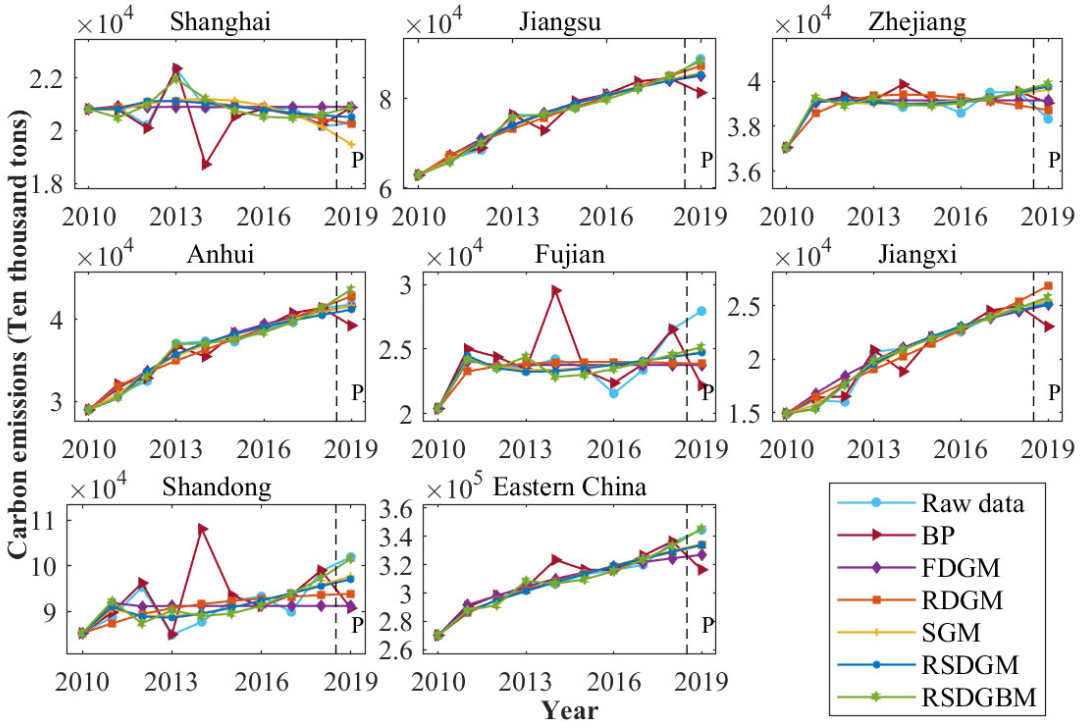


Figure 6. Modeling result curves for all models.

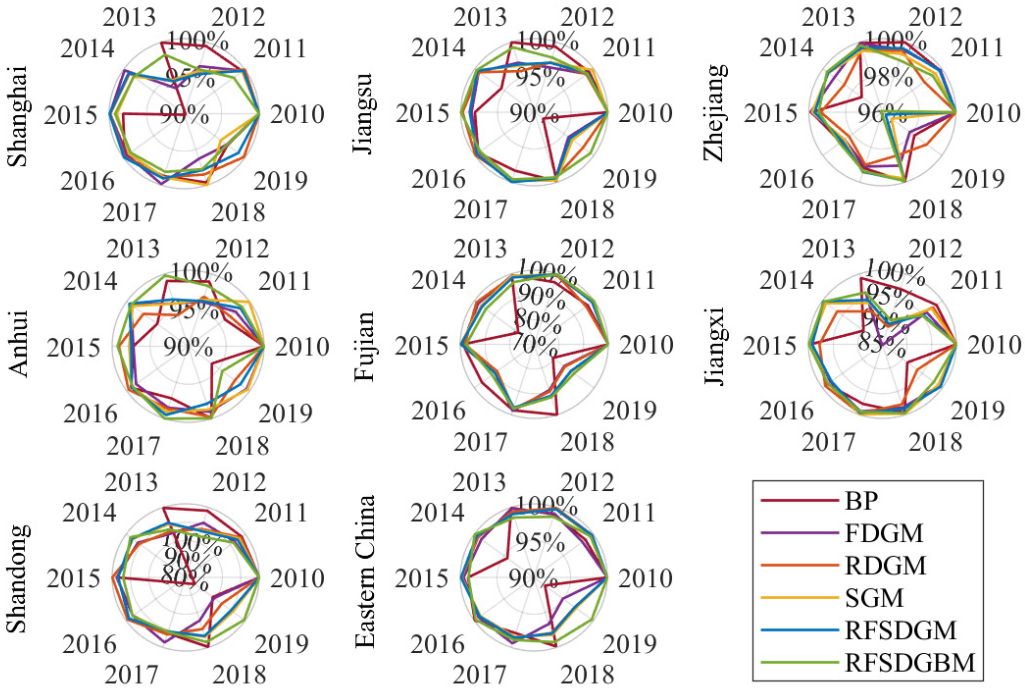


Figure 7. Model fitting results for each model at different time points.

3.4. Carbon Emission Forecasting in the East China Region

As indicated by the comparative analysis in the preceding section, the RSDGBM and RSDGM proposed in this paper show better modeling performance than other models. In order to further confirm the reasoning for breakpoint optimization in the model, both the RSDGM and RSDGBM are used to forecast carbon emissions in the East China region from 2023 to 2030. The RSDGBM designates 2019 as the reference year "*t*" to assess the influence of the COVID-19 outbreak on carbon emissions.

Figure 8 displays the iteration outcomes of the PSO algorithm for both models. The cumulative orders obtained for the RSDGBM and RSDGM models are 1.0098 and 1.0472, respectively. The impressive results of the PSO algorithm in optimizing the cumulative operator with its sleek curves. Overall, the cumulative orders obtained with the PSO algorithm are reasonable and effective for both models. Table 2 displays the modeling inaccuracies of both models, while Figure 9 illustrates the modeling outcome curves. First, the simulation errors of both the RSDGM and RSDGBM are less than 3%, indicating good modeling performance for both models. Second, the MRSPE of the RSDGBM is lower than that of the RSDGM, and the ABMRSPE is only 2.00% after breakpoint t. Figure 9 shows that after time point t, the modeling curve of the RSDGBM better fits the changes in the original data, especially in Zhejiang and Shandong provinces. This reflects the rebound of carbon emissions after the epidemic. In contrast, the modeling result of the RSDGM remains a straight line. This indicates that the RSDGBM can capture the system information after shock and provide good system predictions. The breakpoint optimization method implemented in this study is successful and reasonable.

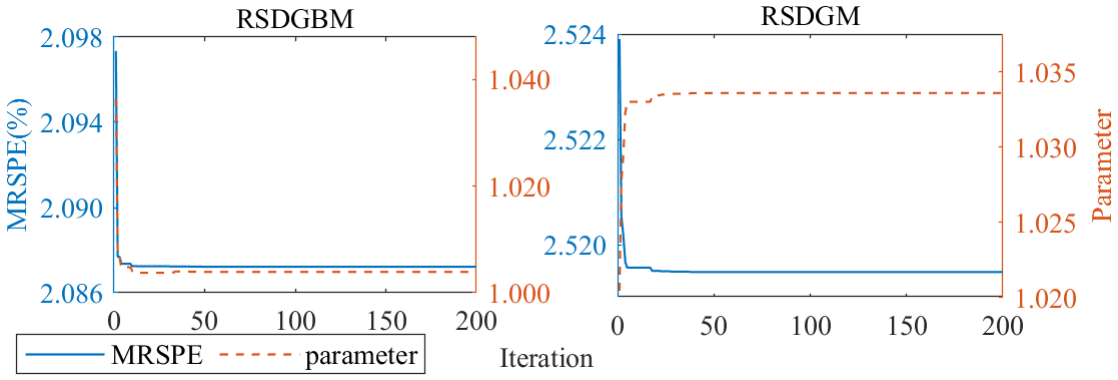


Figure 8. Iteration process of the PSO algorithm in model forecasting.

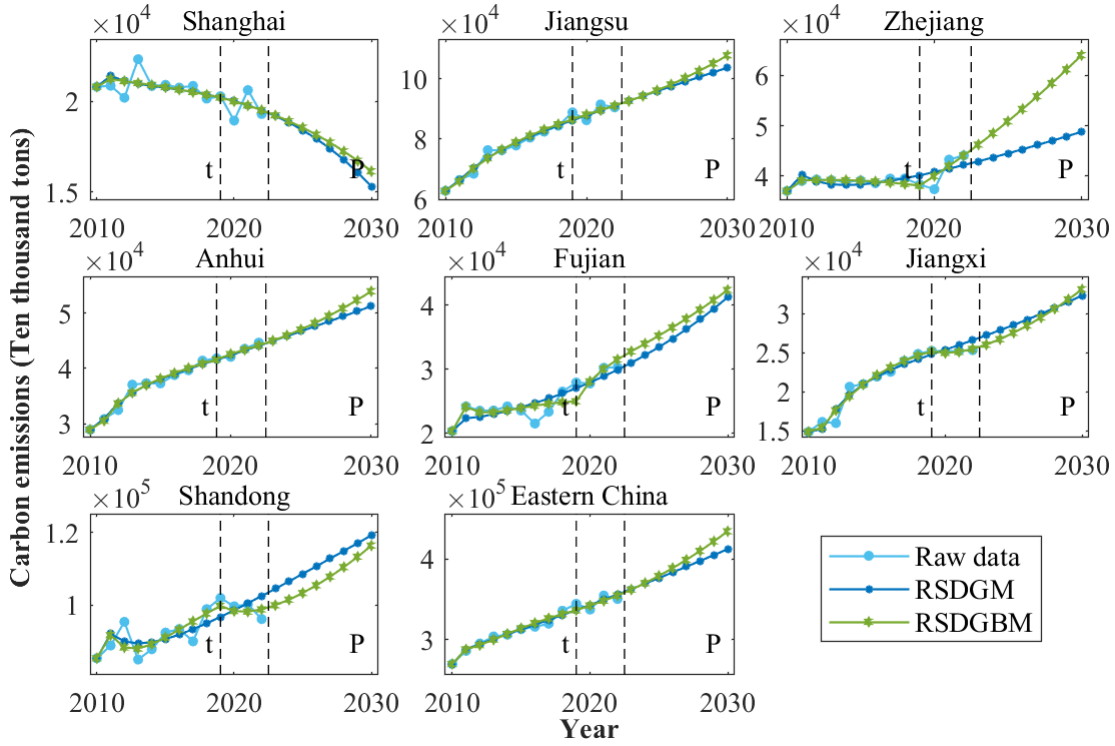


Figure 9. Modeling results of the RDGM and RDSGBM.

Table 2. Modeling errors of the RDGM and RDSGBM.

Model	Accumulated Order R	MRSPE (%)	ABMRSPE (%)
RSDGBM	1.0098	2.09	2.00
RSDGM	1.0472	2.52	2.81

As shown in the analysis above, the RSDGBM outperforms other models and offers more accurate predictions for carbon emissions in the East China region. Therefore, this study adopts the prediction results of the RSDGBM, as presented in Table 3. From a spatial correlation perspective, Shanghai and Zhejiang have negative coefficients, while other regions have positive coefficients. This indicates that higher levels of carbon emissions in nearby areas may result in a reduction of carbon emissions in Shanghai and Zhejiang while causing an increase in carbon emissions in other parts of the region. Jiangsu and Shandong have the highest spatial coefficients, while Shanghai has the lowest spatial coefficient. This suggests that the carbon emissions in the neighboring regions have the most significant influence on Jiangsu and Zhejiang while having the least impact on Shanghai. The forecast indicates that, given the present conditions, carbon emissions in the East China region are projected to rise by around 23.8% by 2030 from the 2022 levels. All regions, except Shanghai, will experience varying degrees of emissions growth. Zhejiang and Fujian are projected to experience significant increases in carbon emissions, with estimated increases of 45.2% and 39.7%, respectively, while Shanghai's carbon emissions are expected to decrease by approximately 16.5% by 2030. Overall, the East China region still faces significant pressure to reduce emissions. Zhejiang and Fujian need to ensure the stabilization of carbon emissions and avoid rebound growth. Jiangsu and Shandong should reduce their dependence on energy for economic development and strive for sustainable economic growth.

Table 3. Modeling results of the RDSGBM (ten thousand tons).

Region	B	2023	2024	2025	2026	2027	2028	2029	2030
Shanghai	−0.01	19,232	18,910	18,553	18,157	17,720	17,239	16,711	16,132
Jiangsu	0.47	92,676	94,360	96,192	98,185	100,345	102,676	105,178	107,851
Zhejiang	−0.08	46,273	48,535	50,887	53,331	55,867	58,494	61,215	64,029
Anhui	0.37	45,036	45,995	47,064	48,242	49,526	50,913	52,401	53,987
Fujian	0.41	32,806	34,023	35,263	36,555	37,910	39,334	40,828	42,392
Jiangxi	0.19	26,051	26,749	27,570	28,499	29,528	30,648	31,853	33,139
Shandong	0.63	99,950	101,485	103,336	105,466	107,850	110,475	113,332	116,414
East China	\	362,024	370,057	378,865	388,434	398,745	409,779	421,518	433,944

4. Conclusions

This study aims to improve the accuracy of the grey model by addressing the shortcomings of the spatial grey model SGM (1,1,m) in background value calculations, parameter calculations, and accumulation methods, taking into account the spatial overflow effect. The RSDGM (1,1,m) is created by merging the distinct version of the spatial grey model with the reverse-accumulation operator. Furthermore, the RSDGM (1,1,m) is optimized with breakpoints based on the impact of the 2020 epidemic, resulting in the RSDGBM (1,1,m,t). Carbon emissions in the East China region are calculated by the energy balance sheets of seven provinces in the region. The RSDGM (1,1,m) and RSDGBM (1,1,m,t) are contrasted with the SGM (1,1,m), FDGM (1,1), RDGM (1,1), and BP models using carbon emissions data from the East China region, confirming the validity of the optimization method proposed in this study. The RSDGM (1,1,m) and RSDGBM (1,1,m,t) are finally used to forecast upcoming carbon emissions in the East China region. The following conclusions can be drawn: (1) The SGM (1,1,m) model can be improved by incorporating discretization and optimization processes along with the reverse-accumulation operator, which can elimi-

nate errors in background value and parameter calculations and decrease computational complexity. (2) The RSDGM (1,1,m) and RSDGBM (1,1,m,t) established in this study outperform the SGM (1,1,m), FDGM (1,1), RDGM (1,1), and BP models, indicating the value of prioritizing new information in spatial analysis. (3) By optimizing the breakpoints of the RSDGM (1,1,m), the RSDGBM (1,1,m,t) is developed to capture the impact of shocks on system development, enabling accurate prediction of systems aftershocks and enhancing the reliability of carbon emissions prediction results. (4) Spatial factors have a greater influence on carbon emissions in Jiangsu and Shandong than in other regions, while carbon emissions in Shanghai and Zhejiang are negatively affected by spatial factors. (5) In general, carbon emissions in the East China region are expected to rise by around 23.8% by 2030 when compared to the levels in 2022. Specifically, Zhejiang and Fujian are expected to experience 45.2% and 39.7% increases in carbon emissions, respectively, while the total in Shanghai is expected to decrease.

The limitation of this study is that it does not discuss the applicability of other accumulation methods on this model, and the model is only applicable to short-term forecasting. Additionally, this study has identified a rebound growth trend for future carbon emissions in Zhejiang and Fujian provinces, but the underlying reasons for this phenomenon are not explored. Investigating the causes of this trend could be a potential research goal.

5. Policy Implication

According to the forecasting results, the East China region still faces significant pressure to reduce carbon emissions. Jiangsu and Shandong continue to be the primary contributors of carbon emissions in the region, with the significant rise in carbon emissions in Zhejiang and Fujian being the main factors driving the increase in carbon emissions in the East China region. To address this issue, efforts should be made in Zhejiang and Fujian to reduce the dependence of economic development on energy, further develop new production strategies, and encourage enterprises to adopt new energy and clean technologies to improve energy efficiency in the production process and reduce carbon emissions. In Jiangsu and Shandong, the government should strengthen carbon emission regulation and encourage enterprises to take emission reduction measures, such as improving energy efficiency and promoting clean energy. At the same time, it is important to encourage enterprises in the East China region to increase their investments in low-carbon technology and innovation to promote innovative development in carbon emission reduction. Provinces should strengthen cooperation, promote the exchange of carbon emission reduction experiences and technologies, learn from the emission reduction policies and strategies implemented in Shanghai, and jointly address carbon emission issues. Strengthening information sharing and technological exchange can promote the joint research, development, and application of carbon emission reduction technologies and achieve a coordinated reduction in carbon emissions. Based on China's opening up to the outside world, local governments can strengthen cooperation with international organizations and other countries, share experiences and technologies, and promote global cooperation and coordinated development to achieve carbon emission reduction.

Author Contributions: Writing—original draft, S.W. and Z.J.; Writing—review and editing, Z.J.; Supervision, X.Y.; Project administration, X.Y. All authors have read and agreed to the published version of the manuscript.

Funding: This research was funded by the Ministry of Education of the People's Republic of China, grant number: 20JZD012.

Institutional Review Board Statement: Not applicable.

Informed Consent Statement: Not applicable.

Data Availability Statement: The data presented in this study are available on request from the corresponding author.

Conflicts of Interest: The authors declare no conflicts of interest.

References

1. Lin, B.Q.; Zhang, Z.H. Carbon emissions in China's cement industry: A sector and policy analysis. *Renew. Sustain. Energy* **2016**, *58*, 1387–1394. [CrossRef]
2. Wang, Y.; Yang, H.X.; Sun, R.X. Effectiveness of China's provincial industrial carbon emission reduction and optimization of carbon emission reduction paths in "lagging regions": Efficiency-cost analysis. *J. Environ. Manag.* **2020**, *275*, 111221. [CrossRef] [PubMed]
3. IPCC. AR4 Climate Change 2007: Synthesis Report. Available online: https://www.ipcc.ch/report/ar4/syr/ (accessed on 24 August 2024).
4. IPCC. AR6 Synthesis Report: Climate Change 2023. Available online: https://www.ipcc.ch/report/sixth-assessment-report-cycle/ (accessed on 24 August 2024).
5. 2022 BP Statistical Review of World Energy Report. Available online: https://www.bp.com (accessed on 5 June 2024).
6. Yang, B.; Bai, Z.; Wang, J. Spatiotemporal dynamic differences of energy-related CO_2 emissions and the related driven factors in six regions of China during two decades. *Environ. Sci. Pollut. Res.* **2022**, *29*, 24737–24756. [CrossRef]
7. Di Sbroiavacca, N.; Nadal, G.; Lallana, F.; Falzon, J.; Calvin, K. Emissions reduction scenarios in the Argentinean Energy Sector. *Energy Econ.* **2016**, *56*, 552–563. [CrossRef]
8. Wang, G.; Feng, Y. Analysis of carbon emission drivers and peak carbon forecasts for island economies. *Ecol. Model.* **2024**, *489*, 110611. [CrossRef]
9. Huang, J.; Li, X.; Wang, Y.; Lei, H. The effect of energy patents on China's carbon emissions: Evidence from the STIRPAT model. *Technol. Forecast. Soc. Chang.* **2021**, *173*, 121110. [CrossRef]
10. Bigerna, S.; Polinori, P. Convergence of KAYA components in the European Union toward the 2050 decarbonization target. *J. Clean. Prod.* **2022**, *366*, 132950. [CrossRef]
11. Ağbulut, Ü. Forecasting of transportation-related energy demand and CO_2 emissions in Turkey with different machine learning algorithms. *Sustain. Prod. Consum.* **2022**, *29*, 141–157. [CrossRef]
12. Deng, J.L. Control problems of grey systems. *Syst. Control Lett.* **1982**, *1*, 288–294.
13. Gao, M.; Yang, H.; Xiao, Q.; Goh, M. A novel method for carbon emission forecasting based on Gompertz's law and fractional grey model: Evidence from American industrial sector. *Renew. Energy* **2022**, *181*, 803–819. [CrossRef]
14. Li, X.; Zhao, Z.; Zhao, Y.; Zhou, S.; Zhang, Y. Prediction of energy-related carbon emission intensity in China, America, India, Russia, and Japan using a novel self-adaptive grey generalized Verhulst model. *J. Clean. Prod.* **2023**, *423*, 138656. [CrossRef]
15. Gu, H.; Wu, L. Pulse fractional grey model application in forecasting global carbon emission. *Appl. Energy* **2024**, *358*, 122638. [CrossRef]
16. Xiong, P.P.; Dang, Y.G.; Yao, T.X.; Wang, Z.X. Optimal modeling and forecasting of the energy consumption and production in China. *Energy* **2014**, *77*, 623–634. [CrossRef]
17. Ding, S.; Dang, Y.G.; Xu, N.; Wei, L. Modeling and optimizing the grey model NGOM (1, 1) for the approximation non-homogenous decreasing series. *Control Decis.* **2017**, *32*, 1457–1464.
18. Ma, X.; Wu, W.; Zhang, Y. Improved GM(1,1) model based on Simpson formula and its applications. *J. Grey Syst.* **2019**, *31*, 33–46.
19. Wang, H.P.; Zhang, Z. A spatial lagged multivariate discrete grey model for forecasting an economy-energy-environment system. *J. Clean. Prod.* **2023**, *404*, 136922. [CrossRef]
20. Wu, L.; Liu, S.; Yao, L.; Yan, S.; Liu, D. Grey system model with the fractional order accumulation. *Commun. Nonlinear Sci. Numer. Simul.* **2013**, *18*, 1775–1785. [CrossRef]
21. Ma, X.; Wu, W.; Zeng, B.; Wang, Y.; Wu, X. The conformable fractional grey system model. *ISA Trans.* **2020**, *96*, 255–271. [CrossRef]
22. Chen, Y.; Lifeng, W.; Lianyi, L.; Kai, Z. Fractional Hausdorff grey model and its properties. *Chaos Solitons Fractals* **2020**, *138*, 109915. [CrossRef]
23. Zhu, H.G.; Liu, C.; Wu, W.Z.; Xie, W.; Lao, T. Weakened fractional-order accumulation operator for ill-conditioned discrete grey system models. *Appl. Math. Model.* **2022**, *111*, 349–362. [CrossRef]
24. Song, Z.M.; Deng, J.L. The accumulated generating operation in opposite direction and its use in grey model GOM (1, 1). *Syst. Eng.* **2001**, *19*, 66–69.
25. Xie, W.; Liu, C.; Wu, W.Z. The fractional non-equidistant grey opposite-direction model with time-varying characteristics. *Soft Comput.* **2020**, *24*, 6603–6612. [CrossRef]
26. Jiang, J.M.; Wu, W.Z. Nonlinear grey Bernoulli Model with fractional-order opposite-direction accumulation and its application. *Math. Pract. Theory* **2021**, *51*, 48–53.
27. Wang, H.P.; Zhang, Z. A novel grey model with fractional reverse accumulation for forecasting natural gas consumption. *Comput. Ind. Eng.* **2023**, *179*, 109189. [CrossRef]
28. Wang, H.P.; Zhang, Z. A novel grey model with conformable fractional opposite-direction accumulation and its application. *Appl. Math. Model.* **2022**, *108*, 585–611. [CrossRef]
29. Zheng, C.; Wu, W.Z.; Xie, W.; Li, Q. A MFO-based conformable fractional nonhomogeneous grey Bernoulli model for natural gas production and consumption forecasting. *Appl. Soft Comput.* **2021**, *99*, 106891. [CrossRef]
30. Ma, X.; Mei, X.; Wu, W.; Wu, X.; Zeng, B. A novel fractional time delayed grey model with Grey Wolf Optimizer and its applications in forecasting the natural gas and coal consumption in Chongqing China. *Energy* **2019**, *178*, 487–507. [CrossRef]

31. Li, N.; Wang, J.; Wu, L.; Bentley, Y. Predicting monthly natural gas production in China using a novel grey seasonal model with particle swarm optimization. *Energy* **2021**, *215*, 119118. [CrossRef]
32. Ding, S.; Li, R.; Tao, Z. A novel adaptive discrete grey model with time-varying parameters for long-term photovoltaic power generation forecasting. *Energy Convers. Manag.* **2021**, *227*, 113644. [CrossRef]
33. Gou, X.; Zeng, B.; Gong, Y. Application of the novel four-parameter discrete optimized grey model to forecast the wastewater discharged in Chongqing China. *Eng. Appl. Artif. Intell.* **2022**, *107*, 104522. [CrossRef]
34. Ye, L.; Yang, D.; Dang, Y.; Wang, J. An enhanced multivariable dynamic time-delay discrete grey forecasting model for predicting China's carbon emissions. *Energy* **2022**, *249*, 123681. [CrossRef]
35. Wang, H.P.; Zhang, Z. Forecasting Chinese provincial carbon emissions using a novel grey prediction model considering spatial correlation. *Expert. Syst. Appl.* **2022**, *209*, 118261. [CrossRef]
36. Gao, M.Y.; Yang, H.L.; Xiao, Q.Z.; Mark, G. COVID-19 lockdowns and air quality: Evidence from grey spatiotemporal forecasts. *Socio-Econ. Plan. Sci.* **2022**, *83*, 101228. [CrossRef]
37. Zhang, Z.; Wang, H.P. A grey breakpoint prediction model and its application in forecasting and policy evaluation. *Eng. Appl. Artif. Intell.* **2023**, *126*, 106784. [CrossRef]
38. Li, S.; Miao, Y.; Li, G.; Ikram, M. A novel varistructure grey forecasting model with speed adaptation and its application. *Math. Comput. Simul.* **2020**, *172*, 45–70. [CrossRef]
39. Wang, Y.; Wang, H.; Zhang, S. Prediction of daily $PM_{2.5}$ concentration in China using data-driven ordinary differential equations. *Appl. Math. Comput.* **2020**, *375*, 125088. [CrossRef]
40. Wu, W.; Ma, X.; Zeng, B.; Lv, W.; Wang, Y.; Li, W. A novel Grey Bernoulli model for short-term natural gas consumption forecasting. *Appl. Math. Model.* **2020**, *84*, 393–404. [CrossRef]
41. Zeng, B.; Tong, M.; Ma, X. A new-structure grey Verhulst model: Development and performance comparison. *Appl. Math. Model.* **2020**, *81*, 522–537. [CrossRef]
42. Han, P.; Cai, Q.; Oda, T.; Zeng, N.; Shan, Y.; Lin, X.; Liu, D. Assessing the recent impact of COVID-19 on carbon emissions from China using domestic economic data. *Sci. Total Environ.* **2021**, *750*, 141688. [CrossRef]
43. Shan, Y.; Ou, J.; Wang, D.; Zeng, Z.; Zhang, S.; Guan, D.; Hubacek, K. Impacts of COVID-19 and fiscal stimuli on global emissions and the Paris Agreement. *Nat. Clim. Chang.* **2021**, *11*, 200–206. [CrossRef]
44. Liang, G.Y.; Liu, Z.Y.; Geng, Z.F. Assessing e-commerce impacts on China's CO_2 emissions: Testing the CKC hypothesis. *Environ. Sci. Pollut. Res.* **2021**, *28*, 56966–56983. [CrossRef] [PubMed]

Disclaimer/Publisher's Note: The statements, opinions and data contained in all publications are solely those of the individual author(s) and contributor(s) and not of MDPI and/or the editor(s). MDPI and/or the editor(s) disclaim responsibility for any injury to people or property resulting from any ideas, methods, instructions or products referred to in the content.